Numerical investigation of blade roughness impact on the aerodynamic performance and wake behavior of horizontal axis wind turbine

Numerical investigation of blade roughness impact on the aerodynamic performance and wake behavior of horizontal axis wind turbine

H H Mian[1], M S Siddiqui[1], L Yang[2] , T Kvamsdal[3] and T Asim[4]

[1]Department of Mechanical Engineering and Technology Management, Norwegian University of Life Sciences, 1432, Ås, Norway
[2]Division of Energy and Sustainability, Cranfield University, UK
[3]Department of Mathematical Sciences, Norwegian University of Science and Technology, Trondheim, Norway
[4]School of Engineering, Robert Gordon University, Aberdeen, UK

E-mail: haris.hameed.mian@nmbu.no , muhammad.salman.siddiqui@nmbu.no , liang.yang@cranfield.ac.uk , trond.kvamsdal@ntnu.no, t.asim@rgu.ac.uk

Abstract. The prolonged operation of wind turbines in harsh offshore environments leads to deterioration and roughness accumulation on the blade surface. This roughness, particularly on the leading edge and other surfaces, can affect the laminar-to-turbulent transition, alter the flow characteristics in the turbine wake and turbulent boundary layer, and become critical for the accurate design and performance analysis of offshore horizontal axis wind turbines (HAWT). This study investigates the effects of blade surface roughness on the aerodynamic performance and wake evolution of the NREL Phase VI wind turbine rotor using the Reynolds-Averaged Navier-Stokes (RANS) technique. First, 2D simulations are validated against experimental data of the S809 airfoil. Then, full-scale 3D simulations of the complete turbine model are conducted with roughness effects to simulate natural conditions. The results show that surface roughness reduces the blade's aerodynamic performance. The rough surface increases the boundary layer thickness, causing flow separation and turbulence, which decrease the lift generated by the blade and increase its drag, resulting in decreased overall blade performance. At higher wind speeds, surface roughness has a negligible effect on turbine performance due to flow separation at the leading edge. The analysis of surface roughness effects on the turbine wake flow indicates that blade roughness positively correlates with wake recovery, where the wake velocity recovers faster with an increase in roughness height.

1. Introduction

Over the past few decades, the number of offshore wind turbines in operation has increased dramatically. Wind turbines are a cost-effective solution for creating environmentally sustainable energy sources [1]. Proper maintenance of the turbine components is critical for consistent energy output throughout its lifetime. The Horizontal Axis Wind Turbine (HAWT) is the most common type of wind turbine used for both onshore and offshore applications. While wind turbines can be constructed and operated in various environments, they are susceptible to contamination from sources such as insects, dirt, dust, and erosion, which can easily accumulate on the turbine blades [2]. In previous studies, researchers have investigated the impact of

surface roughness on the flow over a damaged or rough surface, and several experiments have documented how roughness affects the apparent flow parameters [3]. Estimating complex flow behavior over a rough surface or developing a reliable and efficient computational solution has proven to be challenging. Surface roughness accelerates the laminar-to-turbulent transition process, which has significant practical implications in various flow applications [4]. Low-fidelity models, such as the blade element momentum method, Actuator Line (AL), and Actuator Disk (AD) [5, 6], have limited capacity to estimate three-dimensional flow features, including cross-flow, laminar-to-turbulent boundary layer transition, and surface roughness. Additionally, these models often rely on reduced geometric complexity [7, 8, 9] and reduced order models [10, 11, 12]. In contrast, high-fidelity computational fluid dynamics (CFD) techniques are widely used for wind turbine simulations to more accurately estimate the boundary layer on rotating blades and other unsteady flow features [13, 14, 15, 16, 17].

The NREL unsteady aerodynamics experiment [18] is considered the most comprehensive testing for validating HAWT CFD simulations. The experiment was conducted on the NREL Phase VI wind turbine in the NASA-Ames wind tunnel and has been widely used as a benchmark for comparing CFD simulations in several other studies [19, 20]. CFD simulations for isolated rotors or complete configurations have been carried out using either Reynolds-Averaged Navier-Stokes (RANS) or a hybrid RANS-LES (Large Eddy Simulation) approach [21, 22]. In recent years, researchers have also considered the effects of surface roughness in fully turbulent wind turbine airfoil and wide-blade CFD simulations.

Ferrer and Munduate [23] demonstrated the RANS model's ability to study the effect of leading-edge roughness on the aerodynamic performance of the NREL S814 airfoil. They found that contamination-induced roughness has a more significant impact on aerodynamics than boundary layer tripping and that the RANS simulation demonstrated good agreement with experimental data by predicting the roughness effect at moderate angles of attack. Similarly, Bouhelal *et al.* [24] used RANS-based CFD simulation to investigate the uniform roughness across the entire surface of the Model Experiments in Controlled Conditions (MEXICO) blade. The study used the modified $k-\epsilon$ turbulence model with the sand grain roughness height (k_s). The roughness generally reduces the rotor's overall power at different wind speeds, and in the worst scenario, the reduction in power reaches 35% of the total. Jung and Baeder [25] conducted numerical simulations on the NREL Phase VI rotor and found that the impact of evenly distributed surface roughness on force transition performance depends on the state of the boundary layer. They discovered that coupled flows experienced an 8.3% decrease in performance, while separated flows observed an increase of up to 23.3% when upstream roughness was present. Janiszewska *et al.*[26] found that the S814 airfoil experiences a 25% drop in lift and a 60% increase in drag when exposed to a leading edge grit roughness pattern that imitates a wind turbine field sample. Similar experiments were conducted on 13 different airfoils as part of a larger study by the National Renewable Energy Laboratory (NREL). In a recent study, Kelly *et al.*[27] investigated the impact of blade roughness on wind turbine performance and yearly energy output using CFD-generated polars for NACA4415, S801, and S810 airfoils and the BEM method. They demonstrated that roughened rotor blades cause a performance decline of between 2.9 and 8.6% for a torque-based control method compared to clean rotor blades.

In this study, we began by simulating the S809 airfoil and took into account the impact of surface roughness on flow calculations, with a focus on the boundary layer transition process. Numerical results verification has been conducted through a comprehensive comparison with previously published results by Y. Su *et al.*[25]. Accurately predicting the onset of transition is crucial for understanding the downstream flow history on the blade, especially in the case of leading-edge roughness. Therefore, we used RANS modeling to investigate the effect of leading-edge roughness on turbine aerodynamic performance, taking into account the roughness effect on both the transition process and the turbulent boundary layer. We then extended our

implementation to study the impact of blade roughness on the aerodynamic performance of the NREL Phase VI rotor, a benchmark HAWT model. To account for the roughness effect, we utilized the modified wall function, where the roughness is expressed in terms of the sand grain roughness height (k_s). The simulations were performed using the roughness model that has already been implemented in the CFD software program STAR-CCM+ [28].

2. Governing equations

The present study utilizes a RANS-based CFD model to estimate the flow around an airfoil with transition effects in the boundary layer while considering surface roughness. There are several approaches for accounting for turbine rotation [29], but we have chosen to use the Moving Reference Frame (MRF)[30] approach, which is based on steady-state approximation. This method is straightforward to implement and translates the fluid motion in a rotating frame. Its steady-state solution makes this technique computationally less expensive than other methods like the Sliding Mesh Interface (SMI). For example, in a previous study[31], the use of both MRF and the more accurate SMI method was investigated, and we refer the readers to that paper for more details.

2.1. Reynolds Averaged Navier-Stokes equation

The governing equations for fluid flow are the continuity and conservation of momentum equations (Navier-Stokes equations) [32]. The simulation of turbulent flows is challenging due to the intricate and chaotic nature of turbulence. One key approach to tackling this complexity is the use of RANS equations, which are the fundamental equations derived from the Navier-Stokes equations, adapted to account for the statistical behavior of turbulence. The RANS approach seeks to capture these statistical tendencies by decomposing the flow variables into their mean values and fluctuating components. This decomposition results in a set of equations that describes the evolution of the mean flow properties and their interactions with the turbulent fluctuations. The RANS equations for the conservation of momentum (in vector form for the i-th direction) can be written as follows:

$$\frac{\partial(\rho\overline{u}_i)}{\partial t} + \frac{\partial(\rho\overline{u}_i\overline{u}_j)}{\partial x_j} = -\frac{\partial\overline{P}}{\partial x_i} + \frac{\partial}{\partial x_j}\left[(\mu+\mu_t)\left(\frac{\partial\overline{u}_i}{\partial x_j} + \frac{\partial\overline{u}_j}{\partial x_i}\right)\right] - \frac{\partial\overline{R}_{ij}}{\partial x_j} + \rho g_i$$

Where, ρ is the density of the fluid. $\overline{u}_i$ is the time-averaged velocity component in the i-th direction. P is the pressure and μ is the dynamic viscosity of the fluid. μ_t represents the eddy viscosity (turbulent viscosity).$\overline{R}_{ij}$ are the Reynolds stress terms, which quantify the turbulent transport of momentum and g_i is the acceleration due to gravity in the i-th direction.

The Reynolds stress terms $\overline{R}_{ij}$ arise from the interaction between the fluctuating components of velocity and are typically modeled in terms of turbulence closure models, which involve additional equations to relate them to the mean flow variables. The above equation is a general form of the RANS equation for momentum conservation and can be adapted to specific flow scenarios and coordinate systems.

2.2. Laminar-Turbulent boundary layer transition

The addition of boundary layer transition effects in RANS simulations is made possible by using transition models. Previously, transition modeling relied on an empirical basis [33]. Langtry and Menter [34] further extended the empirical correlation to a free-stream turbulent environment. Intermittency is a fundamental concept in the study of turbulent flows, offering insights into the transition between laminar and turbulent behavior. It quantifies the fraction of time a flow spends in turbulent or non-turbulent states, shedding light on the intermittence of turbulence. In this study, the role of intermittency γ is investigated in understanding turbulent flows and

their impact on the governing equation. The transition onset, which is empirically known in the free stream, is incorporated within the boundary layer dynamics. Based on this flow variable, the scalar intermittency term γ causes the production terms in the Shear Stress Transport (SST) model to be activated, as shown in Equation (1)

$$\frac{\partial(\rho\gamma)}{\partial t} + \frac{\partial(\rho u_j \gamma)}{\partial x_j} = P_\gamma - E_\gamma + \frac{\partial}{\partial x_j}\left[\left(\mu + \frac{\mu_t}{\sigma_f}\right)\frac{\partial(\gamma)}{\partial x_j}\right] \tag{1}$$

In Equation (1), the intermittency concept plays a crucial role in modulating the production terms. The intermittency-dependent variations in these terms stem from the intermittency-induced changes in the flow structure. These changes, influenced by the intermittency fraction, influence the turbulent energy transfer mechanisms and are encapsulated by the intermittency concept. The P and E are the production and destruction terms, respectively, explained in the model development by Menter [33]. To integrate this in STAR-CCM+ solver, Malan *et al.* [35] recommended some minor modifications. To commence the transition locally, the model uses the intermittency concept. The intermittency variable is a scalar term, varying between 0 (representing laminar flow) and 1 (representing turbulent flow).

2.3. Roughness model

The surface roughness in a CFD solver is modeled using the standard wall function as explained in detail by Launder and Spalding [36]. Equation (2) gives the modified wall function.

$$\frac{U_p u^*}{\tau_w/\rho} = \frac{1}{\kappa}\ln\left(E\frac{u^* y_p}{v}\right) - \Delta B \tag{2}$$

Where U_p and y_p are the velocity and height at the cell's center. The term E is the smooth wall's empirical constant with a value of 9.793. ΔB is a roughness function of the dimensionless roughness height of sand particles k_S^+, is defined as:

$$\Delta B = \frac{1}{\kappa}\ln\left(1 - C_S k_S^+\right) \tag{3}$$

k_S is the equivalent height and depending on the value of k_S^+, the roughness regime is defined as: aerodynamically smooth surface $k_S^+ < 2.25$, transitional $2.25 < k_S^+ < 90$ and fully rough surface $k_S^+ > 90$. C_S is the roughness constant (C_S=0.5) for sand grain roughened surfaces. τ_w is the wall shear stress and u^* is the wall friction velocity given in Equation (4):

$$u^* = C_\mu^{1/4} k_p^{1/2} \tag{4}$$

$$k_S^+ = \frac{u^* k_S}{v} \tag{5}$$

In Equation (4), k_p represents turbulent kinetic energy, while C_μ is a constant with a fixed value of 0.09. The basis for modifying the wall function described in Equation (5) stems from Nikuradse's experiments [37] on flow in pipes roughened with sand grains. These experiments demonstrated that the mean velocity distribution is parallel to the logarithmic law distribution near a rough wall. The model has been implemented in Star CCM+ and is used in this study to define the blade surface roughness.

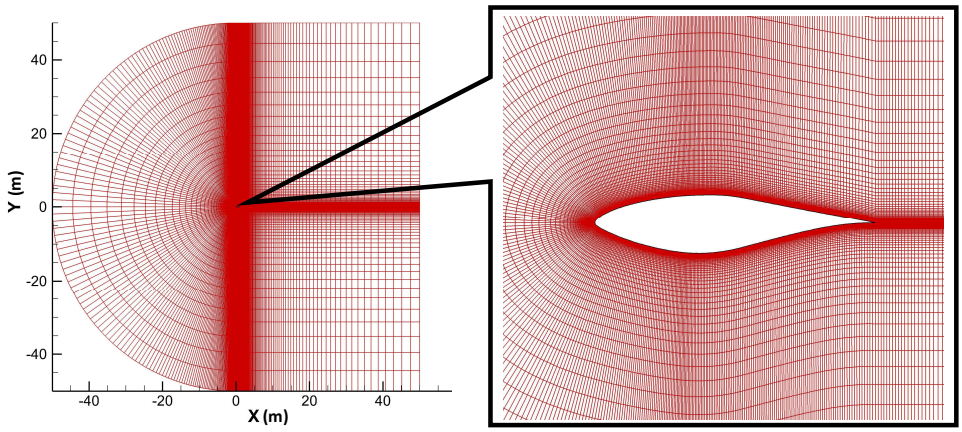

Figure 1. S809 airfoil: C-type structured CFD grid generated for the airfoil resulted in 80,000 quadrilateral cells. The full mesh (left) and zoomed view of the mesh surrounding the airfoil (right).

3. Results and discussion

3.1. S809 airfoil

The S809 airfoil was studied at the Ohio State University subsonic tunnel under both steady and unsteady conditions in the study of [38]. With a thickness of 21%, this airfoil serves as the primary section airfoil for the NREL Phase VI wind turbine blade.

The experimental investigations involved adding leading-edge grit roughness to the airfoil. The roughness was extended on the upper and lower surfaces from the leading edge by almost 11% of the chord length, with an average particle size ratio of 0.0019 relative to the airfoil chord length (k/c). In the CFD simulations, the (k/c) value from the experiment corresponds to the (k_s/c) value for the airfoil model. The maximum Reynolds number in the experiment was 1.5 million, which is also the flow Reynolds number for the simulation. For the 2D computational mesh, shown in Figure 1, a structured grid was used for the S809 airfoil with a blunt trailing edge. The mesh consisted of 400 points defined for the entire airfoil surface and 200 points defined in the normal direction. The initial cell spacing was set at 1×10^{-5}m, such that the value of the wall y^+ was approximately 0.8. To reduce the boundary effects, the far-field boundary was located about 100 chord lengths away. The normal grid spacing was adjusted during the mesh size study to achieve mesh independence.

Initially, simulations were conducted for a clean airfoil to consider both the transition and fully turbulent flow at two different angles of attack, 0^o and 6.2^o. The coefficient of pressure (C_p) obtained from the simulations was compared with the experimental data [39], and good agreement was observed, as shown in Figure 2. It presents an 'intermittency contour,' a visual representation that illustrates the spatial distribution of intermittency within the flow field. An intermittency contour provides a valuable tool for observing the regions of the flow where turbulence intermittency is particularly pronounced or subdued. Each contour line corresponds to a specific intermittency value, allowing us to visualize the evolving patterns of intermittency across the domain. The experimental data also indicated that the transition flow undergoes laminar separation in the boundary layer before reattaching as a turbulent boundary layer, a feature that is not observed in the fully turbulent flow because the boundary layer remains entirely attached. The results from the transition model are appropriate for predicting wind turbine aerodynamics. Figure 3 compares the aerodynamic coefficients (lift and drag) and airfoil performance expressed as the lift-to-drag ratio for both clean and rough surfaces. The results are compared with a previous numerical study and the available experimental data [25]. As indicated

by the results, the current CFD outcomes exhibit strong agreement across the entire range of angles of attack. However, when compared to the experimental data, the numerical results deviate from the measured data after 6°. This discrepancy might arise due to the limitation of the steady two-dimensional flow, which cannot capture the flow separation on the suction side of the airfoil. Both the numerical and experimental results indicate a decrease in performance as the lift-to-drag ratio is reduced for the rough airfoil.

3.2. NREL Phase VI rotor

The study was expanded to include the analysis of turbulent flow over a complete HAWT model for various roughness values. The NREL Phase VI HAWT [40] was designed to investigate research issues such as aerodynamic loads, aeroelasticity, acoustics, and wake-structure interactions. This turbine has been widely used as a benchmark for other small-scale turbines in research facilities, showcasing its effectiveness [41]. The NREL Phase VI HAWT rotor consists of two blades with a diameter of 10.058m and rotates at 72 RPM. It has a linear taper with a blade pitch angle of 3° , and the twist axis is located at 30 % of the chord length. To simulate the turbine numerically, a hybrid-unstructured mesh (illustrated in Figures 4 and 5) was generated with tetrahedral and pyramid cells, along with 35 layers of prismatic cells in the boundary layer region. The blade's surface was represented with a total of 101,229 quadrilateral cells, with an initial wall distance of 1×10^{-5}m, resulting in $y^+ < 1$."

The simulations were conducted for a range of oncoming wind speeds, varying from 7m/s to 25m/s. The surface roughness specifications for the two-dimensional airfoil test case and the wind turbine blade are similar, with a roughness of 10 % of the chord length located from the leading edge for both upper and lower surfaces. Furthermore, the analysis was extended to simulate the turbine for various equivalent sand grain roughness heights. The rotor's thrust and torque estimates were compared with and without leading-edge roughness at different wind speeds to assess the impact of leading-edge roughness on turbine performance. The comparison is presented in Figure 6, where the experimental data [40] is plotted for the clean blade, and reference simulation results are plotted for the rough surface blade.

The comparison results demonstrate that the CFD prediction agrees well with the experiment for wind speeds ranging from 7m/s to 15m/s. However, for the 20m/s case, the turbine's thrust is overpredicted by 11%, and the torque is underpredicted by 13 % when compared with the experimental data. This deviation in the results could be due to the steady-state assumption of

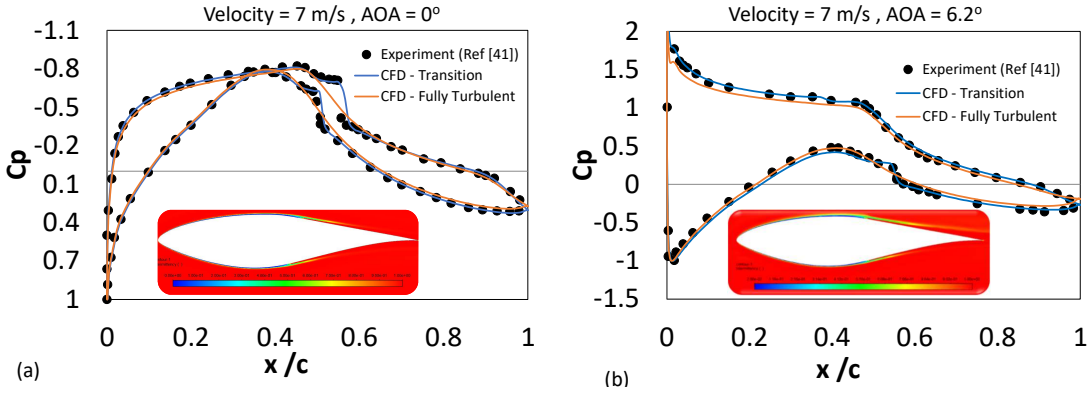

Figure 2. S809 airfoil: Coefficient of pressure (C_p) plot along with the intermittency contours obtained from the transition model at a velocity of 7m/s (a) Angle of attack 0° (b) Angle of attack 6.2°. The comparison has been made between the experimental data (shown by black scatter) and the CFD prediction for transition and fully turbulent flow.

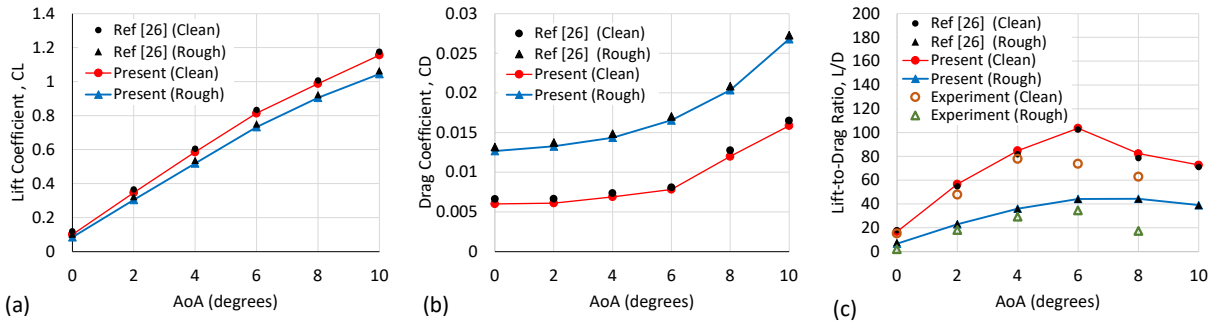

Figure 3. S809 airfoil: Comparison of the predicted aerodynamic parameters for clean and rough surface. (a) Lift coefficient (b) Drag coefficient (c) Lift-to-drag ratio. A comparison has been made between the previous CFD simulation results and the available experimental data.

the simulation in this study, whereas the experimental state is highly unsteady. Furthermore, the thrust and torque estimates for the rough blade are presented in Figure 6(a) and (b), respectively, showing a significant change in predicted torque due to roughness in the range of 10m/s to 15m/s, which may be due to the occurrence of flow separation on the blade. As the wind speed increases, the impact of roughness decreases, and this trend was also observed in previous numerical studies that considered surface roughness. At higher wind speeds, since the flow separates from the leading edge, surface roughness has a negligible effect on turbine performance.

3.2.1. Effect of roughness height variation The presence of surface roughness can significantly impact the flow behavior around a wind turbine blade, leading to changes in boundary layer separation, transition, and aerodynamic performance. This effect creates turbulence in the boundary layer, leading to an earlier separation point and increased drag. The impact of varying the roughness height on the normal and tangential aerodynamic forces acting on the blade is

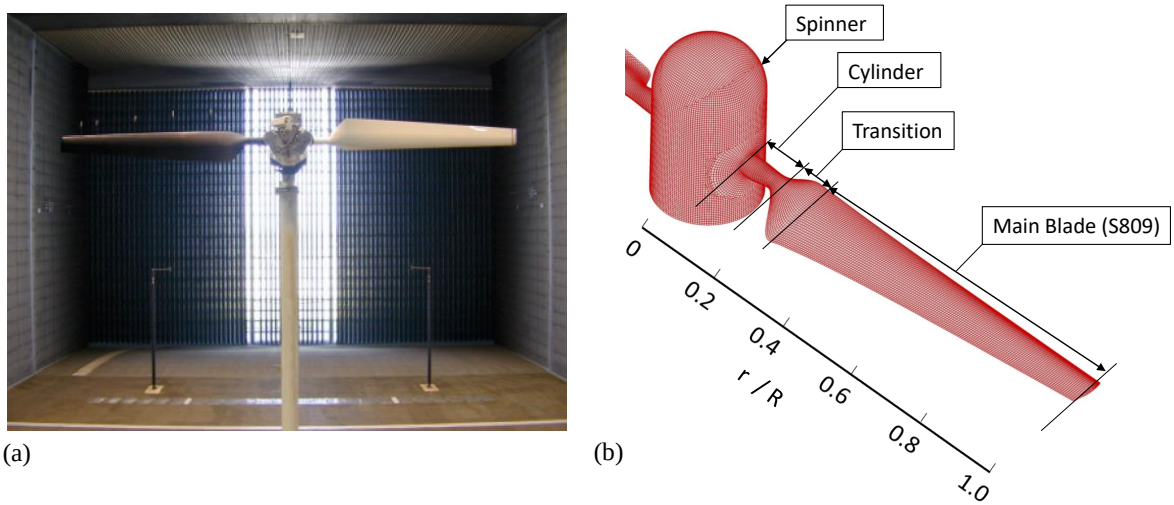

Figure 4. NREL Phase VI: wind turbine blade (a) Actual experimental setup showing the wind turbine placed in a 24.4m × 36.6m wind tunnel test section (b) Isometric view of the surface mesh of the wind turbine blade, showing different turbine sections and a dimensionless scale (r/R) for blade length.

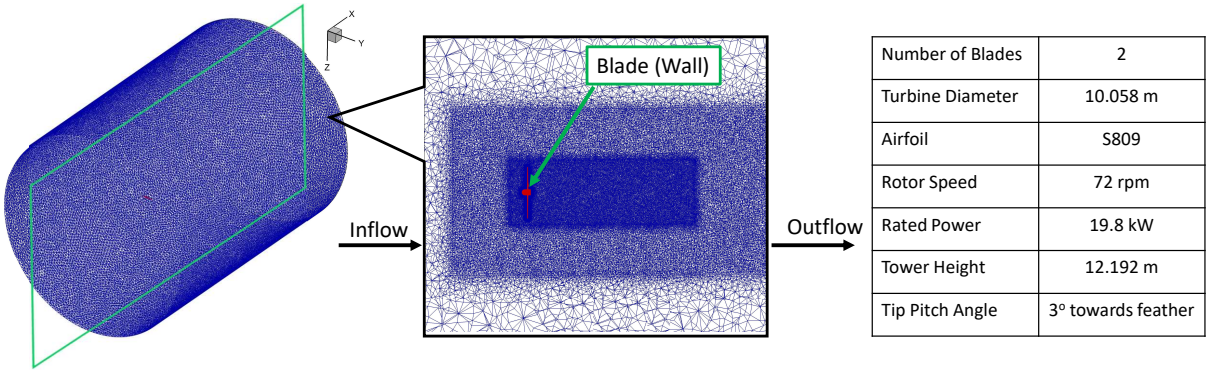

Number of Blades	2
Turbine Diameter	10.058 m
Airfoil	S809
Rotor Speed	72 rpm
Rated Power	19.8 kW
Tower Height	12.192 m
Tip Pitch Angle	3° towards feather

Figure 5. NREL Phase VI: Complete CFD mesh of rotor (left). A section plane is cut to show the mesh density in the interior (mid) with marked boundary conditions and the turbine parameters are given in the table (right)

shown in Figure 7(a) and (b), respectively. The comparison is first made with experimental data [42] available for the clean blade, where some discrepancies at the 30 % and 95 % locations are attributed to modeled geometry (e.g., edge flatness at the tip and blending at the blade transition). However, a reasonable level of agreement is established for the intermediate locations. It is observed that the normal and tangential forces decrease with increasing roughness height. Additionally, the outer region of the blade (r/R >0.5) is more affected by roughness in terms of normal and tangential force. The level of surface roughness is likely to have a significant impact on the stall and flow separation phenomena, as increased roughness can lead to notable alterations in tangential forces. These alterations in tangential forces, induced by roughness, play a key role in influencing the behavior of stall and flow separation.

3.2.2. Effect roughness on the wake Assessment of wind turbine wakes is crucial, particularly for offshore wind farm construction, where one turbine operates in the wake of another. Figure 8 shows line contours of the velocity magnitude indicating wake formation behind the NREL Phase VI rotor, with four regions marked and visualized in a *wake plot*.

The near wake is the closest zone, where the flow velocity is altered by the interaction of the turbine hub or nacelle, and the velocity decreases towards the center. In the transition region, turbulence begins to build up as the tip vortices wear down with expansion in the shear

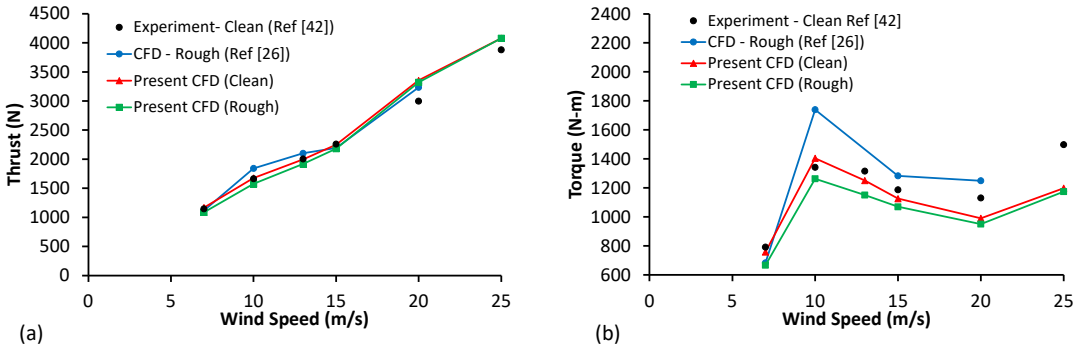

Figure 6. NREL Phase VI: Comparison of the wind turbine performance with the available experimental data (clean blade) and a reference CFD simulation (rough blade): (a) Thrust (N) (b) Torque (N-m)

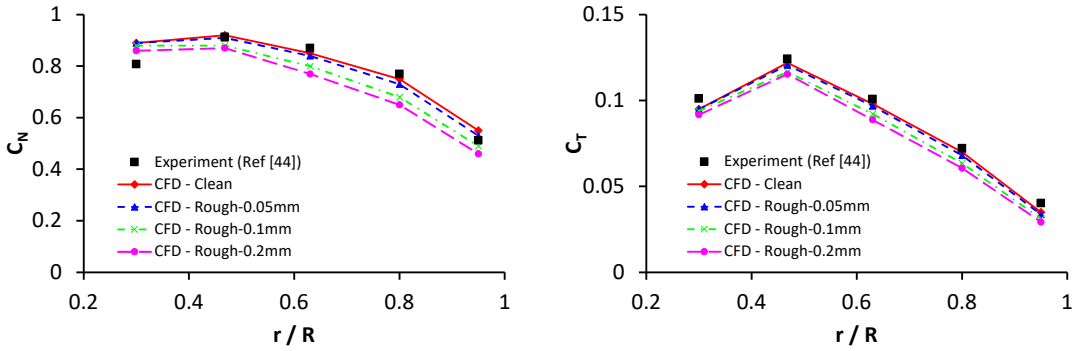

Figure 7. NREL Phase VI: Effect of roughness height on the force coefficients (a) Normal force coefficient (b) Tangential force coefficient. The clean blade comparison is with existing experimental data, and the dotted lines represent the force coefficients for various surface roughness heights.

layer. In the transition phase, the shear layers intersect, and the center-line velocity starts to recover in the decay region. Finally, wake turbulence develops entirely in the far wake zone and is no longer influenced by the turbine. Wind speed is reduced in the far wake, and turbulence intensity increases compared to the undisturbed surrounding flow. This reduction in wind speed and increase in turbulence can significantly affect downstream wind turbines in a wind farm arrangement.

Additionally, it is also observed from the vorticity contours in Figure 9 that the size and strength of the tip vortices decrease as the roughness height is increased. This reduction in the size and strength of the tip vortices can be attributed to the increased mixing between the boundary layer and free stream flow, which leads to a decrease in the pressure difference across the blade span. Therefore, it can be concluded that surface roughness not only affects the aerodynamic performance of the blade but also influences the wake characteristics. Understanding the wake characteristics of wind turbines is crucial in the design and placement of wind farms to maximize energy extraction and minimize wake effects on downstream turbines.

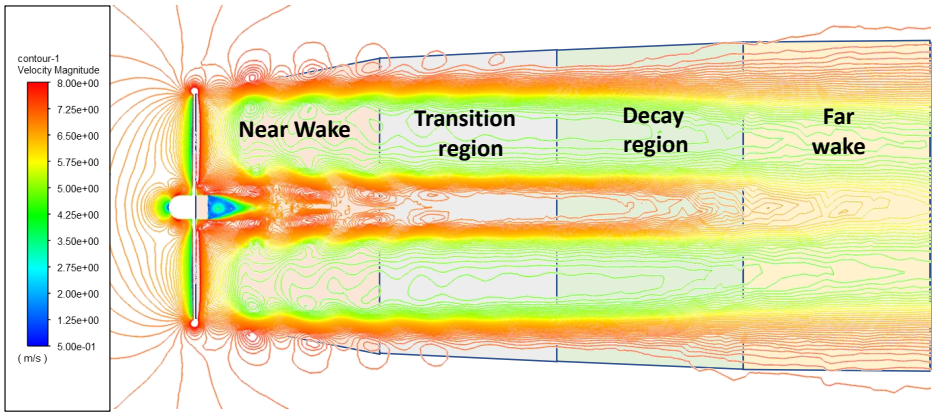

Figure 8. NREL Phase VI: The wake plot showing different wake regions. The line contours of the velocity magnitude are mapped to present the wake flow features.

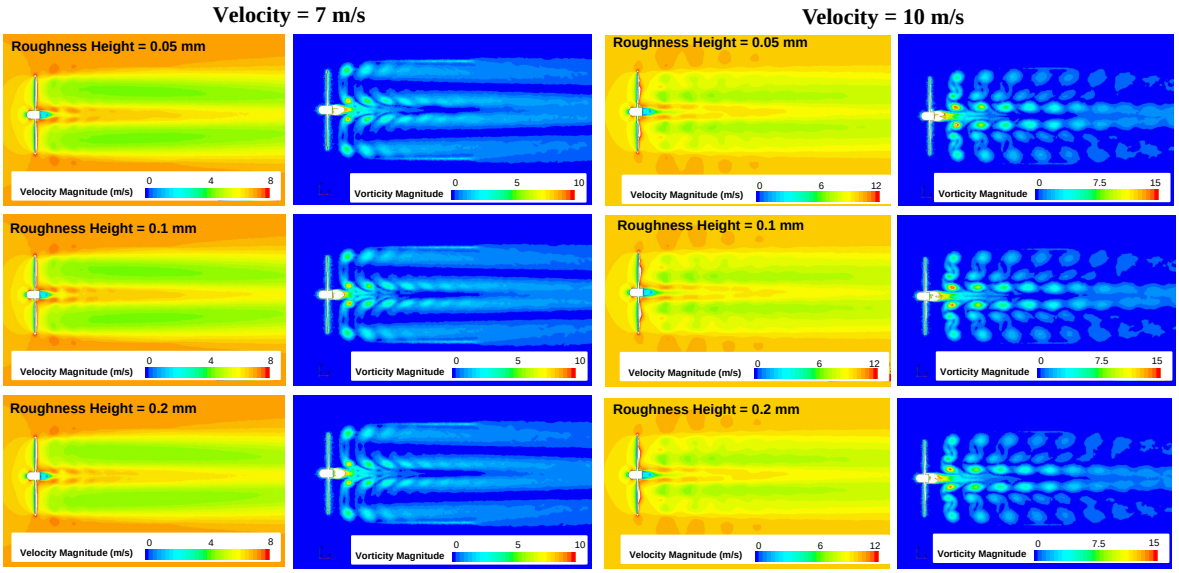

Figure 9. NREL Phase VI: Velocity and the vorticity magnitude plot for free stream wind velocity of 7 m/s and 10 m/s. The contour plots are shown for three different roughness heights (0.05 mm, 0.1 mm, and 0.2 mm)

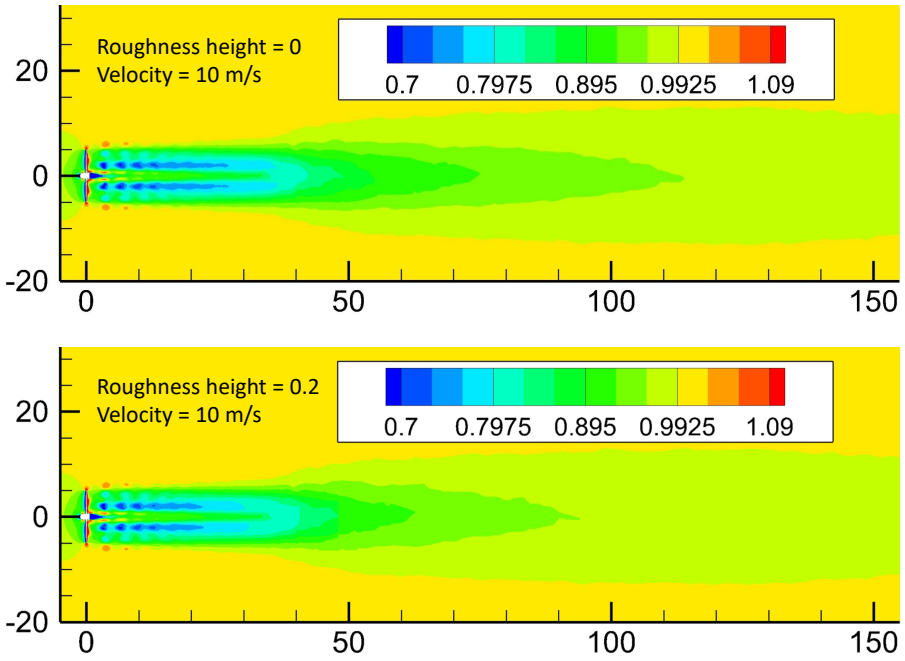

Figure 10. NREL Phase VI: Contours of the normalized free stream velocity (U_x/U_{ref}) for the clean blade (top) and the blade with surface roughness height of 0.2 mm.

4. Conclusion

This study aims to investigate the impact of blade roughness on the performance and wake behavior of a HAWT. Surface roughness is defined in terms of sand grain roughness height, and its effects are analyzed on the S809 airfoil for both fully turbulent and transitional flows. The

study is then extended to the NREL Phase VI rotor, considering both clean and rough blade surfaces.

The current method produces roughness effects on wind turbine aerodynamic performance that are in agreement with experimental data. For the S809 airfoil, the computational and experimental results show a decrease in the lift-to-drag ratio for the rough airfoil. However, due to the steady two-dimensional flow assumption, the numerical results differ slightly from the measured data. Although the CFD predictions and experimental results for the NREL Phase VI wind turbine are in good agreement, some differences are observed. One possible reason for these differences is that the MRF method's steady-state assumption may not be entirely accurate in highly unstable experimental conditions. Additionally, minor changes in blade geometry (between CFD study and experiment) could lead to differences in predicted aerodynamic forces.

The predicted torque for the simulated HAWT is reduced due to roughness, which may be caused by flow separation on the blade. As wind speed increases, the impact of surface roughness on turbine performance decreases, primarily because the flow separates from the leading edge at higher wind speeds. Therefore, surface roughness has a negligible impact on turbine performance under these conditions.

Blade roughness in wind turbine wake flow can increase mixing between the boundary layer and free stream flow, causing turbulence and resulting in faster velocity recovery in the wake compared to a clean blade. This increased mixing due to blade roughness can also lead to increased aerodynamic forces on the turbine blade, which can have implications for wind turbine design and operation.

The model developed in this study would require further investigation to increase the accuracy of roughness effects. Moreover, determining the impact of wind turbine blade roughness on wake velocity recovery is challenging because it depends on various factors, including roughness level, wind speed, turbulence intensity, etc. While the RANS simulation was able to capture the wake behavior caused by blade roughness, future research will incorporate advanced modeling techniques, such as LES or the hybrid RANS-LES model, to further investigate the wake behavior and its associated parameters, such as wake width, velocity minimum, and angle, across various roughness conditions.

Acknowledgement

The authors gratefully acknowledge Mr. Otman Kouaissah of Engineering and Applied Sciences at Università degli Studi di Bergamo, Italy, for providing computational support for StarCCM+ during this research.

References

[1] KAMİL Kaygusuz. Wind power for a clean and sustainable energy future. *Energy Sources, Part B*, 4(1):122–133, 2009.

[2] Mohammad Reza Soltani, Amir Hossein Birjandi, and M Seddighi Moorani. Effect of surface contamination on the performance of a section of a wind turbine blade. *Scientia Iranica*, 18(3):349–357, 2011.

[3] Johann Nikuradse et al. Laws of flow in rough pipes. 1950.

[4] Robert S Downs III, Edward B White, and Nicholas A Denissen. Transient growth and transition induced by random distributed roughness. *AIAA journal*, 46(2):451–462, 2008.

[5] Mandar Tabib, M Salman Siddiqui, Adil Rasheed, and Trond Kvamsdal. Industrial scale turbine and associated wake development-comparison of rans based actuator line vs sliding mesh interface vs multiple reference frame method. *Energy Procedia*, 137:487–496, 2017.

[6] M Salman Siddiqui, Adil Rasheed, Trond Kvamsdal, and Mandar Tabib. Quasi-static & dynamic numerical modeling of full scale nrel 5mw wind turbine. *Energy Procedia*, 137:460–467, 2017.

[7] M Salman Siddiqui, Muhammad Hamza Khalid, Rizwan Zahoor, Fahad Sarfraz Butt, Muhammed Saeed, and Abdul Waheed Badar. A numerical investigation to analyze effect of turbulence and ground clearance on the performance of a roof top vertical–axis wind turbine. *Renewable Energy*, 164:978–989, 2021.

[8] Mandar Tabib, Adil Rasheed, M Salman Siddiqui, and Trond Kvamsdal. A full-scale 3d vs 2.5 d vs 2d analysis of flow pattern and forces for an industrial-scale 5mw nrel reference wind-turbine. *Energy Procedia*, 137:477–486, 2017.

[9] M Salman Siddiqui, Adil Rasheed, Mandar Tabib, and Trond Kvamsdal. Numerical investigation of modeling frameworks and geometric approximations on nrel 5 mw wind turbine. *Renewable Energy*, 132:1058–1075, 2019.

[10] Eivind Fonn, Mandar Tabib, M Salman Siddiqui, Adil Rasheed, and Trond Kvamsdal. A step towards reduced order modelling of flow characterized by wakes using proper orthogonal decomposition. *Energy Procedia*, 137:452–459, 2017.

[11] M Salman Siddiqui, Sidra Tul Muntaha Latif, Muhammad Saeed, Muhammad Rahman, Abdul Waheed Badar, and Syed Maaz Hasan. Reduced order model of offshore wind turbine wake by proper orthogonal decomposition. *International Journal of Heat and Fluid Flow*, 82:108554, 2020.

[12] M Salman Siddiqui, Eivind Fonn, Trond Kvamsdal, and Adil Rasheed. Finite-volume high-fidelity simulation combined with finite-element-based reduced-order modeling of incompressible flow problems. *Energies*, 12(7):1271, 2019.

[13] Niels N Sørensen. Cfd modelling of laminar-turbulent transition for airfoils and rotors using the γ-model. *Wind Energy: An International Journal for Progress and Applications in Wind Power Conversion Technology*, 12(8):715–733, 2009.

[14] M Salman Siddiqui, Trond Kvamsdal, and Adil Rasheed. High fidelity computational fluid dynamics assessment of wind tunnel turbine test. In *Journal of Physics: Conference Series*, volume 1356, page 012044. IOP Publishing, 2019.

[15] M Salman Siddiqui, Adil Rasheed, Trond Kvamsdal, and Mandar Tabib. Influence of tip speed ratio on wake flow characteristics utilizing fully resolved cfd methodology. In *Journal of Physics: Conference Series*, volume 854, page 012043. IOP Publishing, 2017.

[16] Aniket Aranake, Vinod Lakshminarayan, and Karthik Duraisamy. Assessment of transition model and cfd methodology for wind turbine flows. In *42nd AIAA fluid dynamics conference and exhibit*, page 2720, 2012.

[17] M Salman Siddiqui, Adil Rasheed, and Trond Kvamsdal. Validation of the numerical simulations of flow around a scaled-down turbine using experimental data from wind tunnel. *Wind and Structures*, 29(6):405–416, 2019.

[18] M Maureen Hand, DA Simms, LJ Fingersh, DW Jager, JR Cotrell, S Schreck, and SM Larwood. Unsteady aerodynamics experiment phase vi: wind tunnel test configurations and available data campaigns. Technical report, National Renewable Energy Lab., Golden, CO.(US), 2001.

[19] Wenliang Ke, Islam Hashem, Wenwu Zhang, and Baoshan Zhu. Influence of leading-edge tubercles on the aerodynamic performance of a horizontal-axis wind turbine: A numerical study. *Energy*, 239:122186, 2022.

[20] Chengyong Zhu, Yingning Qiu, Yanhui Feng, Wei Zhong, and Tongguang Wang. Rotational effects on the blade flow of a horizontal axis wind turbine under axial and yawed inflow conditions. *Ocean Engineering*, 271:113764, 2023.

[21] M Salman Siddiqui, Adil Rasheed, and Trond Kvamsdal. Numerical assessment of rans turbulence models for the development of data driven reduced order models. *Ocean Engineering*, 196:106799, 2020.

[22] Muhammad Salman Siddiqui, Muhammad Hamza Khalid, Abdul Waheed Badar, Muhammed Saeed, and Taimoor Asim. Parametric analysis using cfd to study the impact of geometric and numerical modeling on the performance of a small scale horizontal axis wind turbine. *Energies*, 15(2):505, 2022.

[23] Xabier Munduate and Esteban Ferrer. Cfd predictions of transition and distributed roughness over a wind turbine airfoil. In *47th AIAA aerospace sciences meeting including the new horizons forum and aerospace exposition*, page 269, 2009.

[24] Abdelhamid Bouhelal, Arezki Smaïli, Christian Masson, and Ouahiba Guerri. Effects of surface roughness on aerodynamic performance of horizontal axis wind turbines. In *The 25th Annual Conference of the Computational Fluid Dynamics Society of Canada, CFD2017-337, University of Windsor*, pages 18–21, 2017.

[25] Yong Su Jung and James Baeder. Simulations for effect of surface roughness on wind turbine aerodynamic performance. In *Journal of Physics: Conference Series*, volume 1452, page 012055. IOP Publishing, 2020.

[26] JM Janiszewska, R Reuss Ramsay, MJ Hoffmann, and GM Gregorek. Effects of grit roughness and pitch oscillations on the s814 airfoil. Technical report, National Renewable Energy Lab.(NREL), Golden, CO (United States), 1996.

[27] Jack Kelly, Christopher Vogel, and Richard Willden. Impact and mitigation of blade surface roughness effects on wind turbine performance. *Wind Energy*, 25(4):660–677, 2022.

[28] W David Pointer. Star ccm+ verification and validation plan. *Consortium for Advanced Simulation of Light Water Reactors, CASL, Oak Ridge, TN, Report No. CASL-U-2016-1198-000*, 2016.

[29] David Hartwanger and Andrej Horvat. 3d modelling of a wind turbine using cfd. In *NAFEMS Conference, United Kingdom*, 2008.
[30] Thanhtoan Tran, Donghyun Kim, and Jinseop Song. Computational fluid dynamic analysis of a floating offshore wind turbine experiencing platform pitching motion. *Energies*, 7(8):5011–5026, 2014.
[31] Kobra Gharali and David A Johnson. Numerical modeling of an s809 airfoil under dynamic stall, erosion and high reduced frequencies. *Applied Energy*, 93:45–52, 2012.
[32] Zhao Zhang, Wei Zhang, Zhiqiang John Zhai, and Qingyan Yan Chen. Evaluation of various turbulence models in predicting airflow and turbulence in enclosed environments by cfd: Part 2—comparison with experimental data from literature. *Hvac&R Research*, 13(6):871–886, 2007.
[33] Florian R Menter, R Langtry, S Völker, and PG Huang. Transition modelling for general purpose cfd codes. In *Engineering turbulence modelling and experiments 6*, pages 31–48. Elsevier, 2005.
[34] Robin B Langtry and Florian R Menter. Correlation-based transition modeling for unstructured parallelized computational fluid dynamics codes. *AIAA journal*, 47(12):2894–2906, 2009.
[35] Paul Malan, Keerati Suluksna, and Ekachai Juntasaro. Calibrating the γ-reθ transition model. *Ercoftac Bulletin*, 80:53–57, 2009.
[36] Brian Edward Launder and Dudley Brian Spalding. The numerical computation of turbulent flows. In *Numerical prediction of flow, heat transfer, turbulence and combustion*, pages 96–116. Elsevier, 1983.
[37] Johann Nikuradse. Stromungsgesetze in rauhen rohren. *vdi-forschungsheft*, 361:1, 1933.
[38] RR Ramsay, M Hoffmann, and G Gregorek. Effects of grit roughness and pitch oscillations on the s809 airfoil: Airfoil performance report, revised (12/99). *National Renewable Energy Laboratory, Golden, CO, Technical Report NREL/TP-442-7817*, 1999.
[39] Dan M Somers. Design and experimental results for the s809 airfoil. Technical report, National Renewable Energy Lab.(NREL), Golden, CO (United States), 1997.
[40] MM Hand, DA Simms, LJ Fingersh, and DW Jager. Jr, cotrel, s. schreck, and sm larwood, 2001," unsteady aerodynamics experiment phase v: Wind tunnel test configurations and available data campaigns'. Technical report, NREL/TP-500-29955.
[41] Mukesh Marutrao Yelmule and Eswararao Anjuri Vsj. Cfd predictions of nrel phase vi rotor experiments in nasa/ames wind tunnel. *International journal of renewable energy research*, 3(2):261–269, 2013.
[42] Andrea G Sanvito, Giacomo Persico, and MS Campobasso. Assessing the sensitivity of stall-regulated wind turbine power to blade design using high-fidelity cfd. In *Turbo Expo: Power for Land, Sea, and Air*, volume 58721, page V009T48A005. American Society of Mechanical Engineers, 2019.